

# Illumination Intensity Dependence of the Photovoltage in Nanostructured TiO<sub>2</sub> Dye-Sensitized Solar Cells

P. Salvador,<sup>\*,†</sup> M. Gonzalez Hidalgo,<sup>†</sup> Arie Zaban,<sup>‡</sup> and Juan Bisquert<sup>§</sup>

*Departament de Matemàtiques i Informàtica, Universitat de les Illes Balears, 07071 Palma de Mallorca, Spain, Department of Chemistry, Bar-Ilan University, Ramat-Gan 52900, Israel, and Departament de Ciències Experimentals, Universitat Jaume I, 12071 Castelló, Spain*

*Received: March 23, 2005; In Final Form: June 7, 2005*

The open-circuit voltage ( $V_{oc}$ ) dependence on the illumination intensity ( $\Phi_0$ ) under steady-state conditions in both bare and coated (blocked) nanostructured TiO<sub>2</sub> dye-sensitized solar cells (DSSCs) is analyzed. This analysis is based on a recently reported model [Bisquert, J.; Zaban, A.; Salvador, P. *J. Phys. Chem. B* 2002, 106, 8774] which describes the rate of interfacial electron transfer from the conduction band of TiO<sub>2</sub> to acceptor electrolyte levels (recombination). The model involves two possible mechanisms: (1) direct, isoenergetic electron injection from the conduction band and (2) a two-step process involving inelastic electron trapping by band-gap surface states and subsequent isoenergetic transfer of trapped electrons to electrolyte levels. By considering the variation of  $V_{oc}$  over a wide range of illumination intensities ( $10^{10} < \Phi_0 < 10^{16}$  cm<sup>-2</sup> s<sup>-1</sup>), three major regions with different values of  $dV_{oc}/d\Phi_0$  can be distinguished and interpreted. At the lower illumination intensities, recombination mainly involves localized band-gap, deep traps at about 0.6 eV below the conduction band edge; at intermediate photon fluxes, recombination is apparently controlled by a tail of shallow traps, while, for high enough  $\Phi_0$  values, conduction band states control the recombination process. The high  $\Phi_0$  region is characterized by a slope of  $dV_{oc}/d \log \Phi_0 \cong 60$  mV, which indicates a recombination of first order in the free electron concentration. The study, which was extended to different solar cells, shows that the energy of the deep traps seems to be an intrinsic property of the nanostructured TiO<sub>2</sub> material, while their concentration and also the density ( $\Theta_t \approx 10^{18}–10^{19}$  cm<sup>-3</sup>) and distribution of shallow traps, which strongly affects the shape of the  $V_{oc}$  vs  $\Phi_0$  curves, change from sample to sample and are quite sensitive to the electrode preparation. The influence of the back-reaction of electrons from the fluorine-doped tin oxide (FTO) conducting glass substrate with electrolyte tri-iodide ions on the  $V_{oc}$  vs  $\Phi_0$  dependence characteristic of the DSSC is analyzed. It is concluded that this back-reaction route can be neglected, even at low light intensities, when its rate (exchange current density,  $j_0$ ), which can vary over 4 orders of magnitude depending on the type of FTO used, is low enough ( $j_0 \leq 10^{-8}$  A cm<sup>-2</sup>). The comparison of  $V_{oc}$  vs  $\Phi_0$  measurements corresponding to different DSSCs with and without blocking of the FTO–electrolyte contact supports this conclusion.

## 1. Introduction

Nanostructured TiO<sub>2</sub> dye-sensitized solar cells<sup>1</sup> (DSSCs) have been proven to be efficient photoelectrochemical devices for the conversion of solar energy into electricity. In DSSCs, the visible light absorber is a monolayer of organic dye molecules covering the internal surface of the nanostructured photoelectrode. Photoexcited electrons at dye molecules are efficiently injected into the conduction band (cb) of the semiconductor. On the other hand, the liquid electrolyte, which makes an excellent contact to the light absorber, allows regeneration of the oxidized dye by electron transfer from reduced, electrolyte dissolved ions. Finally, electrons and holes, which are separated at the TiO<sub>2</sub>–electrolyte interface, are transported through a network of nanosized channels toward the DSSC electrical, outer contacts so that a photocurrent is obtained.

As in other photovoltaic solar cells, a major requirement for high efficiency of photon to electrical energy conversion in a

DSSC is to keep the recombination rate of photogenerated carriers at a low level. The objective of this paper is to gain a better understanding of the recombination mechanism, which, on the other hand, constitutes a major requirement for improving the efficiency of DSSCs.

Excluding electron transfer processes at the fluorine-doped tin oxide (FTO) substrate–electrolyte interface, recombination processes in DSSCs involve different interfacial electron transfer mechanisms with the participation of a wide distribution of band-gap surface states (ss). Figure 1 shows several of the recombination pathways considered by the model. Photoinjected electrons (A), after being transported to the semiconductor (sc) surface (B), may be transferred to empty electrolyte levels, either directly from the cb (isoenergetic process) (C), through ss via intermediate trapping events (D), or by a combination of both processes. Although the existence of a large number of ss is commonly accepted, their distribution in the gap is still under discussion. The two possibilities presented in Figure 1, deep, localized band-gap states (F) and an exponential distribution of shallow band-gap states (G), have been proposed on the basis of electrochemical, photoelectrochemical, and ultraviolet photoelectron spectroscopy (UPS) measurements.<sup>2,3</sup> Although usu-

\* Corresponding author. E-mail: dmipss9@ps.uib.es. On leave from Instituto de Catálisis y Petroleoquímica, CSIC, Spain.

<sup>†</sup> Universitat de les Illes Balears.

<sup>‡</sup> Bar-Ilan University.

<sup>§</sup> Universitat Jaume I.

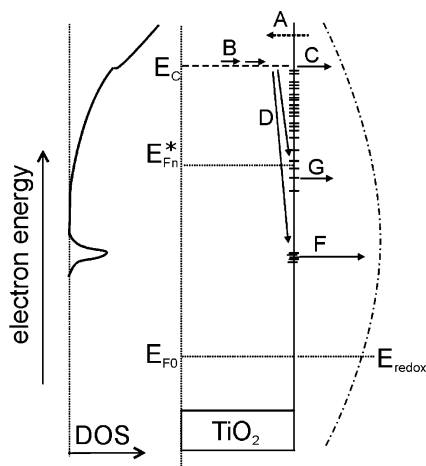


**Figure 1.** Schematic representation according to the model presented here of the steps involved in the in-parallel recombination process between electrons photoinjected in the TiO<sub>2</sub> cb and oxidized electrolyte species. ( $E_{F0}$ ) shows the position of the Fermi level in the dark, equilibrated with the electrolyte redox potential ( $E_{redox}$ ). ( $E_{Fn}^*$ ) is the quasi-Fermi level of electrons under illumination, and  $E_c$  is the conduction band energy. The following steps are indicated: (A) photoinjection; (B) electron transport; (C) electron transfer through the conduction band; (D) capture by surface states; (F) capture by localized, band-gap deep traps; and (G) capture by an exponential distribution of shallow band-gap surface states. On the left side, we show the density of electronic states (DOS) in the TiO<sub>2</sub> nanoparticles and, on the right side, the fluctuating energy levels of oxidized species in solution according to the Gerischer model.<sup>10</sup> The in-parallel recombination process via the FTO substrate is considered in Appendix 3.

ally only one type of these ss is considered, both of them may coexist. Bulk traps at TiO<sub>2</sub> nanoparticles must also be considered, but while they affect the measured lifetime, their contribution to recombination processes under steady-state measurements can be omitted.<sup>4</sup>

The model of Figure 1 shows several recombination pathways in parallel which depend heavily on the occupancy of band-gap ss. Moreover, the rate of electron transfer to the electrolyte depends on the energy match of ss with electrolyte acceptor levels. Therefore, under steady-state conditions, recombination pathways in DSSCs may vary considerably, depending basically on the TiO<sub>2</sub>, cb free electron density,  $n$ .

The essential parameter determining  $n$  under illumination conditions is the quasi-Fermi level,  $E_{Fn}^*$ . On one hand, the value of  $n$  determines the occupancy of band-gap ss at the steady state, so that the net rate of recombination is a function of  $E_{Fn}^*$ . On the other hand,  $E_{Fn}^*$  constitutes a measurement of the open-circuit voltage,  $V_{oc}$ . Under open-circuit conditions, the photogeneration rate, which depends on the illumination intensity,  $\Phi_0$ , is balanced by the recombination rate, so that the type of recombination mechanism can be inferred from the  $V_{oc}$  dependence on  $\Phi_0$ . For example, in the recombination pathway D–G of Figure 1, which involves localized, band-gap deep traps, the rate trapping process D may be written as  $r_t = kn$ , in terms of a rate constant  $k$  and of the free electrons concentration,  $n$  (see eq 9). As full occupancy is approached,  $k$  becomes progressively smaller due to the shortage of vacant defects to accept electrons. Therefore, in order to maintain the generation–recombination balance, a small increase of  $\Phi_0$  involves a substantial raise of  $n$ , so that  $V_{oc}$  raises suddenly. The experimental observation of this sudden increase of  $V_{oc}$ , which is reported and discussed below, allows the recognition of the involvement of localized, band-gap deep traps in the recombination pathway taking place in the range of low illumination intensities. We have recently presented

a detailed model<sup>5</sup> which describes in a general way the  $V_{oc}$  on  $\Phi_0$  dependence that results from the various interfacial mechanisms shown in Figure 1. Here, this model is used in order to describe the experimental steady-state  $V_{oc}(\Phi_0)$  characteristics of DSSCs. Our aim is to be able to discriminate the general mechanisms involved in interfacial electron transfer recombination at DSSCs, as the quasi-Fermi level moves from  $E_{Fn}^* = E_{redox}$  ( $V_{oc} \approx 0$  V), under equilibrium conditions, to the maximum photovoltage,  $\sim 0.7$  V, which is obtained when  $E_{Fn}^*$  approaches the TiO<sub>2</sub> conduction band edge. For this purpose, we have used both our own measurements of  $V_{oc}(\Phi_0)$  and those reported in the literature over a wide range of  $V_{oc}$  values.<sup>7</sup> We show here that the three recombination pathways indicated in Figure 1 are involved in the different DSSCs investigated. Recombination mechanisms via the FTO substrate were shown to be irrelevant to the steady-state  $V_{oc}(\Phi_0)$  characteristics of our DSSC. This new perception allows us to explain the different parts of the  $V_{oc}(\Phi_0)$  curves that can be discerned with the naked eye.

The previous theoretical model<sup>5</sup> has been complemented with more complete expressions when required. The fitting of  $V_{oc}(\Phi_0)$  measurements has allowed us to derive the TiO<sub>2</sub> parameters involved in the recombination processes as well as to discriminate those parameters depending on TiO<sub>2</sub> preparation conditions from those depending on surface treatment methods. These insights provide new tools for tailoring DSSCs' properties.

This paper is composed of several parts. The main text constitutes the application of a general model focused on the recombination mechanisms at the TiO<sub>2</sub>–electrolyte interface, given in ref 5, to the experimental results. Calculations of the photovoltage dependence on the illumination light intensity in specific cases are presented in Appendixes 1 and 2. Furthermore, when this work was first submitted to *The Journal of Physical Chemistry* in September 2003, it was suggested by the reviewers that the role of the conducting glass substrate in the back-reaction of electrons with tri-iodide electrolyte ions cannot be neglected when considering the intensity dependence of the photovoltage of DSSCs where the FTO–electrolyte contact has not been blocked. This point, which has been recently contemplated by Cameron et al.,<sup>6</sup> is considered in Appendix 3, where we demonstrate that the back-reaction of electrons from the substrate with dissolved tri-iodide ions can be frequently ignored, even in DSSCs with uncoated FTO, insofar as the rate of this reaction for FTO substrates is much lower than the back-reaction rate of electrons from surface states (traps) acting as recombination centers.<sup>5</sup> This justifies our experimental observation that no significant difference exists between the  $V_{oc}$  dependence on  $\Phi_0$  of a DSSC with its conducting substrate bare or coated.

## 2. Experimental Section

All chemicals were purchased from Aldrich Chemical Co. and used as received. Nanosized TiO<sub>2</sub> suspensions were synthesized using a titanium tetraisopropoxide precursor. In brief, the titanium tetraisopropoxide dissolved at a 1:1 ratio in 2-propanol was hydrolyzed by acetic acid at pH 2 under rigorous stirring. After this solution was aged overnight, the 2-propanol was evaporated at 82 °C and the suspension was autoclaved at 250 °C for 13 h, resulting in 20 nm crystals.

A conducting glass substrate, 8 Ω/square F-doped SnO<sub>2</sub> (Libby Owens Ford), was cleaned with soap, rinsed with deionized water (18.2 MΩ), and dried in an air stream. The TiO<sub>2</sub> suspension was spread on the conducting substrate with a glass rod, using pieces of adhesive tape as spacers. After the

films were dried under ambient conditions, they were sintered in air at 450 °C for 30 min. The TiO<sub>2</sub> film's thickness, measured with a profilometer (Mitutoyo Co., Suetest SV 500), was 3 μm. To avoid electrochemical reactions via the exposed surface of the FTO, the possible pinholes (FTO areas uncovered with TiO<sub>2</sub>) were electrochemically blocked with an isolating polyphenoxide (PPO) polymer thin layer. The electrochemical deposition was performed at high enough positive potentials so that TiO<sub>2</sub> is not coated. A mixture of 85 mmol of phenol, 85 mmol of tetrabutylammonium hydroxide (TBAOH), and 40 mmol of LiClO<sub>4</sub> in 25 mL of dry ethanol was used as the electrolyte solution for the electrodeposition of isolating phenol on the conducting glass that supports the nanoporous TiO<sub>2</sub>. The electrodeposition was conducted in a three-electrode electrochemical cell using Ag/AgCl as the reference electrode and Pt wire as the counter electrode. The potential of the nanoporous TiO<sub>2</sub> working electrode was scanned at 10 mV s<sup>-1</sup> between 0 and +0.8 V vs Ag/AgCl up to 10 times, while the blocking of the substrate was reflected in the decrease of the polymerization current.

The electrodes were sensitized with the N3 dye [*cis*-di-(isothiocyanato)-bis(4,4-dicarboxy-2,2-bipyridine) ruthenium-(II)] (Solaronic SA Co.). For dye adsorption, the electrodes were immersed overnight in a 0.5 mM solution of dye in absolute ethanol. To avoid the presence of water, the films were heated to 120 °C before immersion in the dye solution.

A sandwich type configuration was employed to measure the performance of the dye-sensitized solar cell, using a F-doped SnO<sub>2</sub> film coated with Pt as a counter electrode. The electrolyte solution consisted of 0.5 M LiI, 0.05 M I<sub>2</sub>, and 2.7 mM 4-*tert*-butylpyridine (TBP) in a 1:1 ratio with acetonitrile-3-methyl-2-oxazolidinone (NMO). The open-circuit photovoltage was recorded using an Ecochemie potentiostat.

Illumination of the cell was performed with a 150 W Xe lamp using a KG3 filter to limit the illumination to the spectrum relevant to the dye-sensitized cell. Light intensity was measured with a calibrated photodiode (UDT Sensors Inc.) by considering the emission lamp spectrum in the experimental range used (400–750 nm). Light intensity was controlled by placing neutral density filters in the illumination path. The short exposure of the cell to the illumination beam and the use of various filters that limit the illumination to the 380–800 nm range ensured that the cell temperature was maintained at a practically constant value.

### 3. Results and Discussion

Figure 2 shows the experimental photovoltage dependence on  $\Phi_0$  of the TiO<sub>2</sub> DSSC previously described. To study the influence of recombination mechanisms via the FTO substrate, the steady-state  $V_{oc}$  dependence on  $\Phi_0$  of the bare electrode was compared with that corresponding to a DSSC coated with a thin blocking PPO layer; no significant differences were observed. This result apparently contradicts those recently obtained by Cameron and Peter<sup>8</sup> concerning transient  $V_{oc}$  measurements. According to these authors, blocking does not apparently affect recombination in the high  $V_{oc}$  range, where interfacial electron transfer at the TiO<sub>2</sub>–electrolyte interface is mediated by the distribution of shallow ss. In contrast, the influence of blocking seems to be significant in the range of low  $V_{oc}$  values, where recombination is mediated by deep TiO<sub>2</sub> traps. Moreover, the changes of the recombination time constant inferred from transient  $V_{oc}$  measurements, even with coated electrodes, clearly indicate that the drastic slope changes generally observed in steady-state  $V_{oc}$  vs  $\Phi_0$  plots at low illumination intensities are not a consequence of recombination via the FTO substrate but via deep, band-gap surface states at the TiO<sub>2</sub>–electrolyte interface.

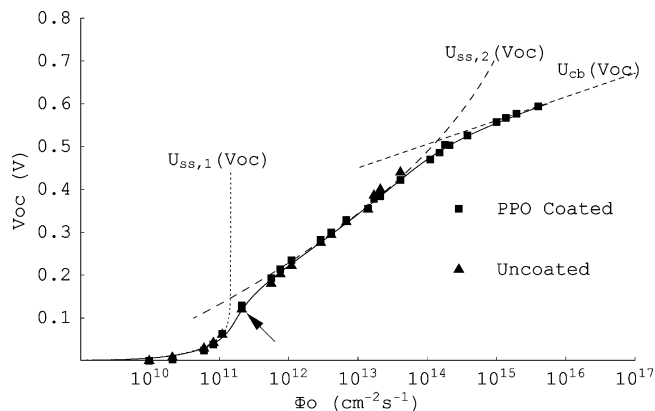


**Figure 2.** Experimental photon flux dependence of the photovoltage obtained under steady-state, open-circuit conditions of the DSSC both bare ( $\blacktriangle$ ) and coated with a blocking PPO polymer thin layer ( $\blacksquare$ ) (see Experimental Section). The arrow indicates the inflection of  $dV_{oc}/d \log \Phi_0$  at low enough  $\Phi_0$ . Also shown is the best fitting of the experimental data according to our recombination model, which combines interfacial electron transfer to oxidized  $I_3^-$  electrolyte species from (a) cb states, according to eq 4, for  $\beta = 1$  ( $U_{cb}(V_{oc})$ ); (b) localized, band-gap deep traps, according to eq 13 ( $U_{ss,1}(V_{oc})$ ); and (c) an exponential distribution of band-gap ss just below  $E_c$ , according to eq 19 ( $U_{ss,2}(V_{oc})$ ). The full line  $\Phi_0(V_{oc})$  is the result of considering simultaneously the three recombination pathways ( $U_{ss,1}(V_{oc}) + U_{ss,2}(V_{oc}) + U_{cb}(V_{oc})$ ). Common fitting parameters:  $\alpha = 3 \times 10^3 \text{ cm}^{-1}$ ,  $d = 3 \times 10^{-4} \text{ cm}$ ,  $E_c - E_{redox} = 0.7 \text{ eV}$ ,  $\lambda = 0.6 \text{ eV}$ ,  $\sigma_n \nu = 1.6 \times 10^{-9} \text{ cm}^3 \text{ s}^{-1}$ ,  $c_{ox}/c_{red} = 10^{-1}$ , and  $N_c = 4 \times 10^{20} \text{ cm}^{-3}$ . Exclusive fitting parameters: (a)  $e_{cb}^{cb} = 8 \times 10^{-1} \text{ s}^{-1}$ ; (b)  $N_t = 2.9 \times 10^{15} \text{ cm}^{-3}$ ,  $e_{ox} = 5 \times 10^{-2} \text{ s}^{-1}$ ,  $e_{red} = 2.2 \times 10^{-1} \text{ s}^{-1}$ ,  $E_{ox} - E_t = 0.52 \text{ V}$ ,  $A = 2.37 \text{ s}^{-1}$ , and  $E_t - E_{redox} = 0.075 \text{ eV}$ ; (c)  $A_{ox} = A_{red} = 5 \text{ s}^{-1}$ ,  $\alpha' = 0.3$ , and  $\Theta_t = 8 \times 10^{17} \text{ cm}^{-3}$ . It must be stated that, according to the definition of the demarcation level (the energy level at which  $e_{ox} = e_r$  and  $f \approx 1/2$ ),<sup>3</sup>  $E_d \approx E_{redox} + kT \log(2e_{ox}/e_t)$ , and in our case,  $E_d \approx E_{redox}$ . This means that the filling factor  $f(E)$  for the exponential distribution of ss is described by the Fermi–Dirac statistics around the quasi-Fermi level,  $E_{Fn}^*$ , so that a good approach for the recombination rate,  $e_r$ , is that given by eq 18.

Three well-defined regions can be distinguished in the steady-state  $V_{oc}$  vs  $\Phi_0$  plots of Figure 2: (a) for values of  $\Phi_0$  between  $10^{10}$  and  $2 \times 10^{11} \text{ cm}^{-2} \text{ s}^{-1}$ ,  $dV_{oc}/d \log \Phi_0$  increases monotonically from  $\sim 10$  to  $\sim 230 \text{ mV}$ ; (b) from  $\sim 2 \times 10^{11} \text{ cm}^{-2} \text{ s}^{-1}$  up to  $\sim 2 \times 10^{14} \text{ cm}^{-2} \text{ s}^{-1}$ ,  $dV_{oc}/d \log \Phi_0$  starts to decrease to reach a constant value of  $\sim 120 \text{ mV}$ ; (c) finally, for  $\Phi_0 > 2 \times 10^{15} \text{ cm}^{-2} \text{ s}^{-1}$ , the slope of  $V_{oc}$  vs  $\Phi_0$  decreases again to a value near  $60 \text{ mV}$ . Similar behavior has been observed by Fisher et al.<sup>7</sup> Especially interesting is the fact that  $V_{oc}$  appears to depend linearly on  $\log \Phi_0$ , for  $\Phi_0$  values varying over about 2 orders of magnitude in the intermediate high intensity range ( $10^{14} \geq \Phi_0 \geq 10^{12} \text{ cm}^{-2} \text{ s}^{-1}$ ). An analogous linear dependence has been described by Schlichthörl et al.<sup>9</sup> However, the values of  $dV_{oc}/d \log \Phi_0$  found by Fisher et al.<sup>7</sup> and Schlichthörl et al.<sup>9</sup> in this linear range are about  $85\text{--}90 \text{ mV}$ , which contrasts with the slope of  $120 \text{ mV}$  found by us. In the apparent absence of direct evidence about the influence of recombination via the FTO substrate on the steady-state  $V_{oc}$  dependence on  $\Phi_0$ , we will assume that recombination takes place mainly at the TiO<sub>2</sub>–electrolyte interface. Therefore, the dependence of  $V_{oc}$  on  $\Phi_0$  will be analyzed in light of the recombination model we have recently proposed.<sup>5</sup>

On the basis of the Gerischer model for weak electronic semiconductor–electrolyte interaction,<sup>10</sup> we assume interfacial electron transfer from the TiO<sub>2</sub> to electrolyte energy levels ( $I_3^-$ ) to take place isoenergetically with the participation of cb energy levels and band-gap ss.<sup>5</sup>

Under open-circuit conditions, the photovoltage is defined as the shift experienced by the Fermi level under illumination

( $E_{Fn}^*$ ) with respect to its value under equilibrium conditions in the dark ( $E_{Fn} = E_{redox}$ )

$$V_{oc} = \frac{E_{Fn}^* - E_{redox}}{q} = \left[ \frac{E_c}{q} - kT \ln \left( \frac{N_c}{n} \right) \right] - \left[ \frac{E_c}{q} - kT \ln \left( \frac{N_c}{n_0} \right) \right] = \frac{kT}{q} \ln \left( \frac{n}{n_0} \right) \quad (1)$$

where  $N_c$  is the effective density of cb electronic states,  $E_c$  is the lower limit of the cb, and  $n$  and  $n_0$  are the concentration of cb free electrons under illumination conditions and at equilibrium in the dark, respectively.

**3.1. Direct Recombination from cb States.** At steady state, under open-circuit conditions, the continuity equation for cb free electron density takes the form

$$\frac{\partial n}{\partial t} = G - U_{cb} = 0 \quad (2)$$

where  $G$  represents the electron photogeneration rate, i.e., the rate of injection of electrons into the cb from photoexcited dye molecules ( $G \approx \eta \Phi_0 (1 - e^{-\alpha d})/d$ , where  $\eta$  ( $\sim 1$ ) is the photo-injection efficiency,  $\alpha$  ( $\sim 10^3 \text{ cm}^{-1}$ ) is the absorption coefficient of dye molecules, and  $d$  is the absorbing  $\text{TiO}_2$  film thickness), and  $U_{cb}$  is the back-reaction rate of electrons from the  $\text{TiO}_2$  conduction band to the electrolyte; observe that, while  $\Phi_0$  ( $\text{cm}^{-2} \text{ s}^{-1}$ ) represents the incident photon flux per unit of surface area,  $G$  ( $\text{cm}^{-3} \text{ s}^{-1}$ ) represents the photon flux absorbed per unit of volume ( $G \approx \alpha \Phi_0$  for  $d \leq 3 \mu\text{m}$ , while  $G \approx \Phi_0/d$  for  $d \leq 10 \mu\text{m}$ ).

In general, for the case of nonlinear recombination, we have that

$$U_{cb} \approx e_{ox}^{cb} (n^{\beta'} - n_0^{\beta'}) \quad (3)$$

where  $\beta'$  represents the reaction order in the concentration of cb free electrons and  $e_{ox}^{cb}$  is the interfacial transfer frequency. The combination of eqs 1–3 can be written as

$$V_{oc} = \frac{2.3kT}{q} \log \left( \frac{G}{n_0^{\beta'} e_{ox}^{cb}} + 1 \right)^{1/\beta'} \quad (4)$$

so that for  $U \gg e_{ox}^{cb} n_0^{\beta'}$  we have that

$$V_{oc} = \frac{2.3kT}{q} \log(G)^{1/\beta'} - \log n_0^{\beta'} e_{ox}^{cb} \quad (5)$$

and

$$\frac{dV_{oc}}{d \log \Phi_0} = \frac{2.3}{\beta'} \frac{kT}{q} \quad (5)$$

Equation 5 establishes a linear dependence of  $V_{oc}$  on  $\log \Phi_0$  for values of  $\Phi_0 \gg (n_0^{\beta'} e_{ox}^{cb})/\eta\alpha$  with a constant slope of  $(2.3/\beta')(kT/q)$  V. A maximum slope of  $(dV_{oc}/d \log \Phi_0) \approx 60 \text{ mV}$  is obtained for  $\beta' = 1$ .

The experimental results of Figure 2, as well as those reported by Fisher et al.<sup>7</sup> and Schlichthörl et al.,<sup>9</sup> are clearly incompatible with an interfacial electron transfer mechanism exclusively involving cb states, as  $\beta'$  depends on  $\Phi_0$ . Only for high enough illumination intensities ( $\Phi_0 \geq 2 \times 10^{15} \text{ cm}^{-2} \text{ s}^{-1}$ ), a value of  $(dV_{oc}/d \log \Phi_0) \approx 60 \text{ mV}$  is obtained in Figure 2 and is, therefore, compatible with a direct electron transfer mechanism from cb states to  $\text{I}_3^-$  oxidized electrolyte species. This linear behavior for  $\beta' = 1$  in eq 4 has not been reported by other

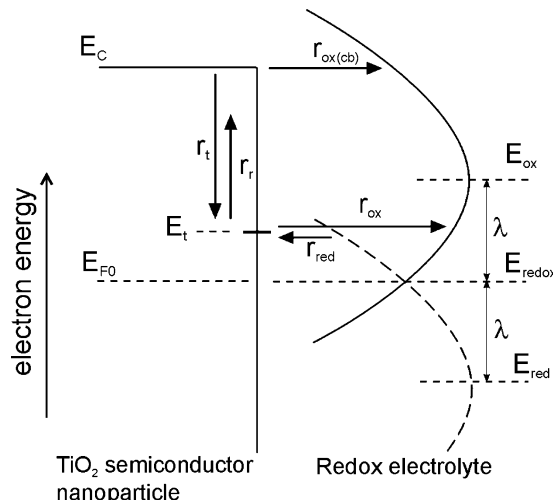


**Figure 3.** Energy diagram schematically showing isoenergetic interfacial electron transfer between both cb and band-gap surface states and fluctuating energy levels of the electrolyte permeating semiconductor  $\text{TiO}_2$  nanoparticles in a DSSC according to the Gerischer model.<sup>10</sup> ( $E_c$ : low energy level of the semiconductor conduction band.  $E_{F0}$ : Fermi level at equilibrium in the dark.  $E_c$ : energy of band-gap ss.  $E_{redox}$ : electrolyte redox energy.  $E_{ox}$ ,  $E_{red}$ : most probable energy levels for oxidized and reduced electrolyte species ( $E_{redox} = 1/2(E_{ox} + E_{red})$ ).  $\lambda$ : reorganization energy.  $r_t$ ,  $r_r$ : net rate for electron trapping and detrapping by ss.  $r_{ox}$ ,  $r_{red}$ : rate for interfacial electron transfer front and back between ss and oxidized and reduced electrolyte species, respectively.  $r_{ox}(cb)$ ,  $r_{red}(cb)$ : net rate for interfacial electron transfer, front and back, between the cb and energy levels of oxidized and reduced electrolyte species, respectively.)

authors, probably because in their experiments they did not reach high enough  $\Phi_0$  values.

**3.2. Recombination Involving Band-Gap ss.** Interfacial electron transfer can take place in a two-step process involving ss. In the first step, electrons are transferred inelastically from cb states to ss (electron trapping process) at a rate  $r_t$ . In the second step, electrons trapped at ss are isoenergetically transferred, according to the Gerischer model,<sup>10</sup> to fluctuating energy levels of oxidized, electrolyte dissolved species at a rate  $r_{ox}$ . As schematized in Figure 3, ss trapped electrons can also be released back (detrapped) to the cb at a rate  $r_r$  and electroreduced electrolyte species be reoxidized by isoenergetic transfer of electrons to ss at a rate  $r_{red}$ . Band-gap ss can be considered either to have a unique energy  $E_t$ <sup>11–14</sup> or to be distributed energetically from  $E_c$  along the band gap.<sup>15–20</sup>

The interfacial electron transfer rate is obtained according to the Marcus–Gerischer fluctuating energy model for weak interaction between dissolved electron acceptors ( $\text{I}_2$  species) and the  $\text{TiO}_2$  surface.<sup>5</sup> This model is not valid if the dissolved electron acceptor is strongly adsorbed. Although the electrochemical behavior of iodine at the  $\text{TiO}_2$  surface in acetonitrile is not known to the best of our knowledge, considering the polar character of acetonitrile, it should interact with the  $\text{TiO}_2$  surface more strongly than iodine, so that the application of the Marcus–Gerischer model seems suitable. In principle, one could test simple models for interfacial electrochemistry such as the Butler–Volmer equation. However, in a separate paper,<sup>22</sup> we have reported the remarkable finding that the electron lifetime in a DSSC increases in a certain range of open-circuit voltages when the driving force for recombination (i.e., the quasi-Fermi level) increases. This behavior cannot be explained by a monotonic dependence such as that predicted by the Butler–Volmer equation and is rather characteristic of the Marcus inverted region. The results presented here are, in general, consistent with the Marcus–Gerischer model.

(a) *Recombination Kinetics Involving Monoenergetic ss.* Let us consider a density  $N_t$  of ss with a unique energy  $E_t$ , as in Figure 3. The continuity equation under open-circuit conditions then becomes<sup>5</sup>

$$\frac{\partial n}{\partial t} = G - U_{ss,1} = G - r_t + r_r = 0 \quad (6)$$

If we denote the filling factor of ss as  $0 \leq f \leq 1$ , the density of trapped electrons will be  $n_t = N_t f$ , so that the balance equation for the occupation of ss becomes

$$N_t \frac{df}{dt} = r_t + r_{red} - r_r - r_{ox} \quad (7)$$

Under steady-state conditions ( $\partial n/\partial t = \partial f/\partial t = 0$ ), eqs 6 and 7 lead to

$$G = U_{ss,1} = r_t - r_r = r_{ox} - r_{red} \quad (8)$$

The rate of electron trapping by ss can be written as<sup>5</sup>

$$r_t = N_t(1 - f)e_t \quad (9)$$

where  $e_t = \sigma_n \nu n$  is the trapping frequency ( $\sigma_n$  is the electron capture cross section of traps and  $\nu$  the thermal velocity of cb free electrons).

On the other hand, the detrapping rate is

$$r_r = N_t f e_r \quad (10)$$

with the detrapping frequency,  $e_r = N_c \nu \exp[(E_t - E_c)/kT]$ .

Since the Marcus–Gerischer model involves a one-electron process and the iodide–tri-iodide system is a two-electron process, it has been assumed that the rate-determining step of the global recombination process is the initial step  $I_2 + e^- \leftrightarrow I_3^-$ .<sup>7</sup> Therefore, it can be written that<sup>5</sup>

$$r_{ox} = N_t f e_{ox} = N_t f A_{ox} \exp\left[-\frac{(E_t - E_{ox})^2}{4\lambda kT}\right] \quad (11)$$

and

$$r_{red} = N_t(1 - f)e_{red} = N_t(1 - f)A_{red} \exp\left[-\frac{(E_t - E_{red})^2}{4\lambda kT}\right] \quad (12)$$

where  $A_{ox}$  ( $s^{-1}$ ) =  $A_{c_{ox}}$  and  $A_{red}$  ( $s^{-1}$ ) =  $A_{c_{red}}$ ,  $E_{ox}$  and  $E_{red}$  are the most probable energy levels for oxidized ( $I_2$ ) and reduced ( $I_2^-$ ) electrolyte species, respectively,  $\lambda$  is the reorganization energy ( $E_{ox} - E_{red} = 2\lambda$ , see Figure 3), and  $A$  ( $cm^{-3} s^{-1}$ ) is a preexponential factor. The solution of rate eq 8 is described in detail in Appendix 1, and the following result is obtained for the relationship between  $V_{oc}$  and  $G(\Phi_0)$ :

$$V_{oc} = \frac{kT}{q} \ln \left[ \frac{e_{ox} + e_r}{e_{t_0}} \frac{G + N_t e_{red}}{N_t e_{ox} - G} - \frac{e_{red}}{e_{t_0}} \right] \quad (13)$$

A plot of  $V_{oc}$  vs  $G$  from eq 13 is shown in Figure 4. It can be seen that both  $V_{oc}$  and  $dV_{oc}/d \log G$  increase monotonically with  $G$ . Moreover, as  $G \rightarrow N_t e_{ox}$  (i.e., as  $f \rightarrow 1$ ), both  $V_{oc}$  and  $dV_{oc}/d \log G$  increase very rapidly ( $V_{oc} \rightarrow \infty$ ), as outlined in the Introduction. However, as the ss become filled ( $f \approx 1$ ), interfacial electron transfer from cb states becomes predominant, so that, according to eq 3,  $dV_{oc}/d \log G$  suddenly decreases to a constant value of  $1/\beta$ , not shown in Figure 4 (for details see Figure 4 of ref 5).

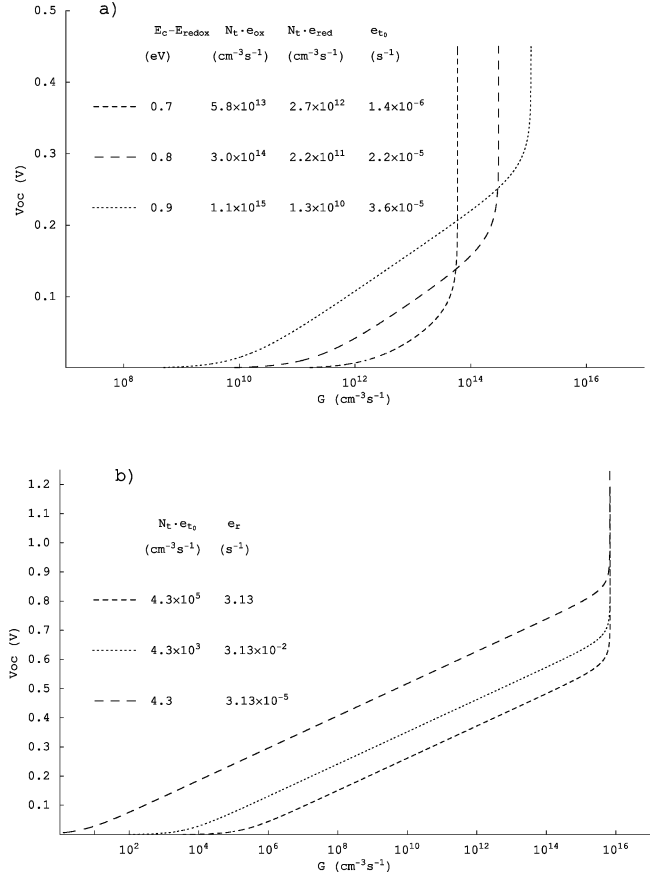


**Figure 4.** Photovoltage dependence on the absorbed photon flux, according to eq 13, for isoenergetic, interfacial electron transfer between localized, band-gap deep traps and oxidized electrolyte species, for different values of (a)  $E_c - E_{redox}$ ,  $N_t e_{ox}$ ,  $N_t e_{red}$ , and  $e_{t_0}$  ( $\sigma_n \nu = 1.6 \times 10^{-9} cm^3 s^{-1}$  and  $e_r = 3.13 s^{-1}$ ; observe that, as  $e_{ox} \approx e_r$  and  $e_{ox} \gg e_{red}$ , the linear range of  $V_{oc}$  vs  $\Phi_0$  takes place within the illumination range  $N_t e_{ox} > G > N_t e_{red}$ ) and (b)  $N_t e_{t_0}$  and  $e_r$  ( $E_c - E_{redox} = 1.2 eV$ ,  $N_t e_{ox} = 6.8 \times 10^{15} cm^{-3} s^{-1}$ , and  $N_t e_{red} = 3.2 \times 10^5 cm^{-3} s^{-1}$ ; observe that, as  $e_{ox} \gg e_r$  and  $e_{ox} \gg e_{red}$ , the linear range of  $V_{oc}$  vs  $\Phi_0$  takes place within the illumination range  $N_t e_{ox} > G > N_t e_{t_0}$ ). Common parameters:  $N_t = 2.9 \times 10^{15} cm^{-3}$ ,  $N_c = 4.0 \times 10^{20} cm^{-3}$ ,  $\lambda = 0.6 eV$ ,  $A_{ox} = 2.37 s^{-1}$ , and  $E_c - E_t = 0.62 eV$ .

It is interesting to realize the existence of a linear stretch with a slope  $dV_{oc}/d \log \Phi_0 \approx 60 mV$  in Figure 4. This behavior is implicit in eq 13, which can be rewritten as  $n/n_0 = aG + b$ , with  $a = (e_{ox} + e_r)/(N_t e_{tr}(e_{ox} + e_{red}))$  and  $b = e_{red}/e_{tr}((e_{ox} + e_r)/(e_{ox} + e_{red}) - 1)$ . Both for  $b = 0$  and for  $G \gg b/a$ ,  $n/n_0 \approx aG$ , so that  $V_{oc} \approx 2.3kT(\log a + \log G)$  and  $dV_{oc}/d \log \Phi_0 \approx 60 mV$ . The condition  $b = 0$  occurs when both  $e_r \approx e_{red}$  and  $e_{ox} \gg e_{red}$  and also when  $e_{ox} \geq e_r$ . In these cases,  $n/n_0 \approx G/N_t e_{t_0}$ , which means that for  $n > n_0$   $G$  must be greater than  $N_t e_{t_0}$  and a linear stretch must appear in the plot of  $V_{oc}$  vs  $\log G$ , within the photon flux interval  $N_t e_{ox} > G > N_t e_{t_0}$  (see Figure 4b). On the other hand, for  $e_{ox} \gg e_{red}$  and  $e_r \gg e_{ox}$ , the condition  $G \gg b/a = (N_t e_{red}(e_r - e_{red}))/((e_{ox} + e_r))$  becomes  $G \gg N_t e_{red}$ , so that a linear dependence with slope  $dV_{oc}/d \log \Phi_0 \approx 60 mV$  appears in the range  $N_t e_{ox} > G > N_t e_{red}$  (see Figure 4a).

(b) *Recombination Kinetics Involving a Distribution of Band-Gap ss.* An exponential tail of band-gap ss near the cb (Figure 2) is a common property of amorphous semiconductors (sc's), which has also been invoked for explaining transport properties in nanostructured TiO<sub>2</sub> electrodes.<sup>9,15–20</sup> A typical exponential, continuous distribution of ss with concentration  $N_t(E)$  is, for instance,<sup>21</sup>

$$N_t(E) = \frac{\Theta_t}{kT_c} \exp\left[-\alpha' \left(\frac{E_c - E}{kT}\right)\right] \quad (14)$$

where  $\Theta_t$  represents the total volume density of states,  $T_c$  is a characteristic temperature that defines the tail shape (broadening) of the exponential distribution, and  $\alpha' = T/T_c$  ( $T$  is the absolute temperature).

According to eq 8, the recombination rate under open-circuit conditions becomes<sup>5</sup>

$$U_{ss,2} = \int_{E_v}^{E_c} N_t(E) \{f(E) e_{ox}(E) - [1 - f(E)] e_{red}(E)\} dE \quad (15)$$

where the steady-state occupancy of each energy level,  $f(E)$ , varies between 0 and 1 and the electron transfer probabilities  $e_{ox}(E)$  and  $e_{red}(E)$ , as in the case of eqs 11 and 12, have the following Gaussian form:

$$e_{ox}(E) = A_{ox} \exp\left[-\frac{(E - E_{ox})^2}{4\lambda kT}\right] \quad (16)$$

$$e_{red}(E) = A_{red} \exp\left[-\frac{(E - E_{red})^2}{4\lambda kT}\right] \quad (17)$$

According to the definition of the demarcation level,  $E_d$  (the energy level where  $e_{ox} = e_r$ ),<sup>5</sup> those ss above  $E_d$  can be considered to be in thermal equilibrium with the cb;  $f(E)$  is then described by the quasi-Fermi level,  $E_{Fn}^*$  (i.e., only the ss below  $E_{Fn}^*$  participate in the recombination process), so that eq 15 becomes

$$U_{ss,2} = \int_{E_{redox}}^{E_{Fn}^*} N_t(E) e_{ox}(E) dE \quad (18)$$

As we will show in sections 3.3 and 3.4, this approximation is justified in our case, as  $E_d \approx E_{redox}$  and, therefore,  $e_r/e_{ox} > 1$  for  $E > E_{redox}$ . Using this assumption, it is possible to transform eq 18 into a closed expression by means of the quadrature procedure that is described in Appendix 2. The following explicit dependence of  $V_{oc}$  on  $G$ , in terms of the error function and the inverse error function, is found:

$$V_{oc} = \sqrt{b} \operatorname{inverf}\left[\frac{G}{\alpha'} \operatorname{erf}\left(\frac{-a}{\sqrt{b}}\right)\right] + a \quad (19)$$

Figure 5a shows a plot of  $V_{oc}$  vs  $G$  according to eq 19, for typical values of the intervening parameters. The corresponding plot of  $V_{oc}$  vs  $G$  in logarithmic scale is shown in Figure 5b. As expected, for  $G = 0$ ,  $V_{oc} = 0$  and  $dV_{oc}/d \log G$  scales up monotonically with  $G$ . For small enough values of  $G$  ( $G \leq 10^{18} \text{ cm}^{-3} \text{ s}^{-1}$ ),  $dV_{oc}/d \log G$  increases slowly, although it increases very rapidly ( $dV_{oc}/d \log G \rightarrow \infty$ ) for  $G \geq 10^{19} \text{ cm}^{-3} \text{ s}^{-1}$ . Moreover,  $dV_{oc}/d \log G$  appears apparently constant, i.e.,  $V_{oc}$  depends linearly on  $\log G$ , in the range  $10^{16} \geq G \geq 10^{14} \text{ cm}^{-3} \text{ s}^{-1}$ . In this range, the Fermi level is at the maximum of the combined density of states, i.e., at  $2\lambda\alpha'$  above the  $E_{ox}$  level. Indeed this is the behavior to be expected from eq A2.3 within the photon flux interval  $E_{ox} + 2\lambda\alpha' - 4.5(2kT\lambda)^{1/2} \leq G \leq E_{ox} + 2\lambda\alpha' - (2.8kT\lambda)^{1/2}$ , which depends on the electrolyte parameters  $E_{ox}$  and  $\lambda$  and on the semiconductor parameter  $\alpha'$ . It can be concluded, therefore, that the broadening of the exponential distribution of ss,  $\alpha'$ , is the only semiconductor parameter which affects the slope of the  $V_{oc}$  vs  $G$  plot. As can be seen in Figure 6a for  $G < 10^{18} \text{ cm}^{-3} \text{ s}^{-1}$ , an increase of  $\alpha'$

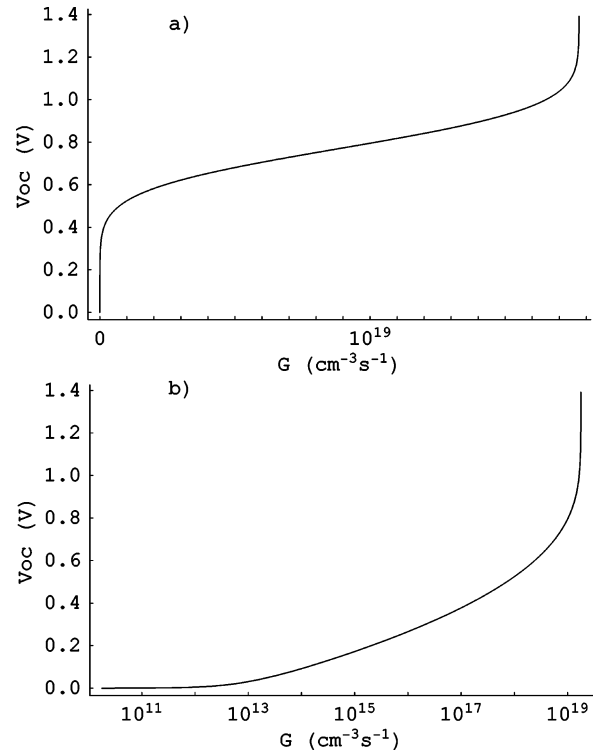


**Figure 5.** Typical dependence of  $V_{oc}$  on the absorbed photon flux, according to eq 19. (a) Linear scale of  $G$ ; (b) logarithmic scale of  $G$  ( $E_c - E_{redox} = 0.9 \text{ eV}$ ,  $\lambda = 0.5 \text{ eV}$ ,  $A_{ox} = 8 \text{ s}^{-1}$ ,  $\alpha' = 0.27$ , and  $\Theta_t = 10^{19} \text{ cm}^{-3}$ ). Observe that  $dV_{oc}/d \log G$  increases monotonically with  $G$ . Moreover, due to the Gaussian behavior of eq A2.3 (Appendix 2), an almost linear dependence of  $V_{oc}$  on  $\log G$  appears within the range  $10^{17} \geq G \geq 10^{14} \text{ cm}^{-3} \text{ s}^{-1}$ , while, for  $G > 10^{19} \text{ cm}^{-3} \text{ s}^{-1}$ ,  $dV_{oc}/d \log G \rightarrow \infty$ .

for constant values of  $A_{ox}$  and  $\Theta_t$  produces a decrease of  $dV_{oc}/d \log G$  and an increase of  $V_{oc}$ . This tendency is reverted for  $G > 10^{18} \text{ cm}^{-3} \text{ s}^{-1}$ , in such a way that for  $G \approx 5 \times 10^{18} \text{ cm}^{-3} \text{ s}^{-1}$   $V_{oc}$  becomes independent of  $\alpha'$ . This is just the behavior predicted by eq 14, according to which an increase of  $\alpha'$  leads to an increase of the number of band-gap ss with energy  $E_{ox} > E > E_c$ . On the other hand, an increase of  $\alpha'$  involves an increase of  $dN_t(E)/dE$ , so that according to eq 18, for constant values of  $G$  and  $e_{ox}$ ,  $V_{oc}$  must increase. Moreover, since  $dV_{oc}/dG$  is proportional to  $dN_t(E)/dE$ , which in turn is proportional to  $\alpha'$ ,  $dV_{oc}/dG$  must increase with  $\alpha'$ . Figure 6b and c shows the influence of  $\Theta_t$  and  $A_{ox}$  on the plot of  $V_{oc}$  vs  $G$ . As predicted by eq A2.2, the increase of  $\Theta_t$  and  $A_{ox}$  produces a decrease of  $V_{oc}$ .

**3.3. Model Fitting of the  $V_{oc}$  Experimental Dependence on  $\Phi_0$ .** None of the three pathways of the interfacial electron transfer considered in the recombination model, neither direct recombination via cb states nor indirect recombination via band-gap ss (localized, band-gap deep traps or a tail of band-gap shallow traps), can separately fit the experimental results of Figure 2 in the whole illumination range ( $10^{10} \leq \Phi_0 \leq 10^{16} \text{ cm}^{-2} \text{ s}^{-1}$ ). However, as shown in Figure 2, a reasonably good fitting can be obtained by combining the three recombination pathways. In fact, for low light intensities ( $\Phi_0 \leq 10^{11} \text{ cm}^{-2} \text{ s}^{-1}$ ), the experimental data can be reasonably well fitted by assuming recombination via localized, band-gap deep traps localized  $\sim 0.6 \text{ eV}$  below  $E_c$  ( $U_{ss,1}(V_{oc})$ ). For  $5 \times 10^{13} \geq \Phi_0 \geq 10^{12} \text{ cm}^{-2} \text{ s}^{-1}$ , an exponential distribution of band-gap ss (shallow traps), just below  $E_c$  ( $U_{ss,2}(V_{oc})$ ), with a broadening parameter  $\alpha = 0.3$ , fits the experimental results well. Finally, for  $\Phi_0 \geq 10^{15} \text{ cm}^{-2} \text{ s}^{-1}$ , a good fitting is obtained by assuming direct recombination from cb states ( $U_{cb}(V_{oc})$ ), with a reaction order  $\beta' = 1$  (see eq 3), as a constant slope of  $dV_{oc}/d \log \Phi_0 \approx$

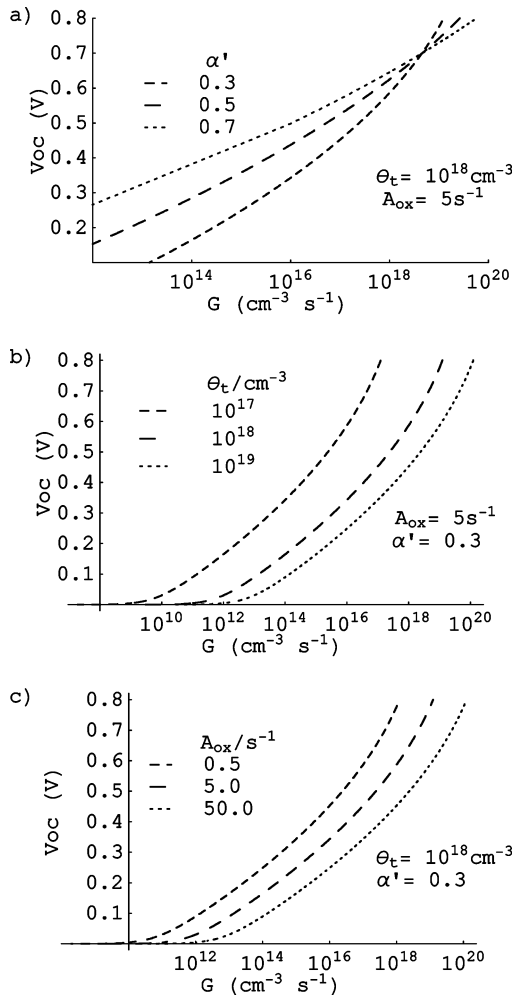


**Figure 6.** Typical plot of  $V_{oc}$  vs  $\log G$ , according to eq 19, for different values of (a) the broadening parameter of the exponential distribution of band-gap ss,  $\alpha'$ ; (b) the density of ss,  $\Theta_t$ ; and (c) the preexponential factor,  $A_{ox}$ , of the interfacial electron transfer frequency,  $e_{ox}$ , according to eq 16. Common parameters:  $E_c - E_{redox} = 0.7 \text{ eV}$ ,  $\lambda = 0.6 \text{ eV}$ ,  $\sigma_n \nu = 1.6 \times 10^{-9} \text{ cm}^3 \text{ s}^{-1}$ ,  $c_{ox}/c_{red} = 0.1$ , and  $N_c = 4 \times 10^{20} \text{ cm}^{-3}$ . Observe that  $\alpha'$  is the only sc parameter affecting the slope of  $V_{oc}$  vs  $\log G$ .

60 mV is observed. A global fitting is obtained by addition of the three recombination pathways, i.e.,

$$\Phi_0(V_{oc}) = U_{ss,1}(V_{oc}) + U_{ss,2}(V_{oc}) + U_{cb}(V_{oc}) \quad (20)$$

A possible criticism for this model is that it has a large number of adjustable parameters and that, unless independent measurements of some of them are made, the fitting becomes inefficient. However, it must be pointed out that the large number of parameters is intrinsic to the complex system under study and, therefore, cannot be obviated by the model. Attention must be paid mainly to the ability of the model to explain the drastic slope change (inflection of  $dV_{oc}/d \log \Phi_0$ ) observed experimentally in the steady-state  $V_{oc}$  vs  $\Phi_0$  plots at low enough  $\Phi_0$  values (see Figure 2 and Figure S1 in the Supporting Information) and not to its ability to fit intervening parameters.

Equation 18 has been used for the calculation of the recombination rate under open-circuit conditions. This takes into account that ss participating in the recombination process are in thermal equilibrium with the conduction band, which is only true for ss above the demarcation level,  $E_d$ , i.e., when  $e_r > e_{ox}$ .<sup>5</sup> As can be seen in Figure 7, where  $e_r(E)$  and  $e_{ox}(E)$  are calculated from eqs A1.2 and 16, respectively, with the same fitting

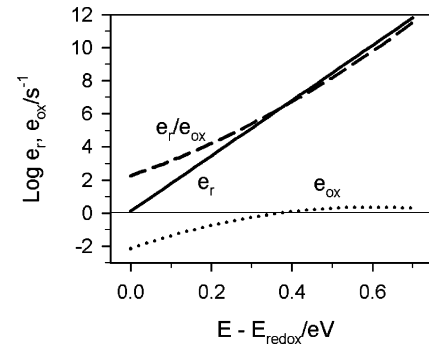


**Figure 7.** Logarithmic plot of  $e_{ox}$ ,  $e_r$ , and  $e_r/e_{ox}$  vs  $E$ , according to eq A1.2 (Appendix 1) and eq 16, for  $E_c > E > E_{redox}$  and the same fitting parameters used in Figure 2.

parameters used in Figure 2,  $e_r \gg e_{ox}$  for  $E_c > E > E_{redox}$ , so that the use of eq 18 is justified.

Experimental evidence of deep traps 0.5–0.8 eV below  $E_c$  exists in the literature.<sup>11–14</sup> These traps have been attributed to TiO<sub>2</sub> lattice defects associated with incompletely coordinated Ti<sup>4+</sup> surface ions.<sup>14</sup> On the other hand, an exponential tail of ss below  $E_c$ , which has been attributed to surface disorder of the crystal lattice,<sup>15</sup> has been invoked for explaining dispersive transport properties<sup>17–20</sup> and surface recombination processes in nanoporous TiO<sub>2</sub>.<sup>16,17,19</sup>

A similar dependence of  $V_{oc}$  on  $\Phi_0$  as that shown in Figure 2, but with lower values of  $V_{oc}$ , has been reported by Fisher et al.<sup>7</sup> These experimental data are also nicely fitted with our recombination model, as shown in Figure S1 of the Supporting Information. The best fitting in this case is obtained by keeping those parameters which are less sensitive to electrode preparation ( $N_c$ ,  $E_t - E_{redox}$ ,  $\lambda$ ,  $\sigma_n \nu$ ,  $e_{ox}$ ,  $e_{red}$ ,  $e_{t0}$ ,  $e_r$ , and  $e_{oc}^{cb}$ ) constant, while increasing those parameters which are more sensitive to the electrode synthesis ( $N_t$  and  $\Theta_t$  increase by about 2 orders of magnitude, and  $\alpha$  increases from 0.3 to 0.5). It must be emphasized that, also in the case of the results of Fisher et al.,<sup>7</sup> a sudden decrease of  $dV_{oc}/d \log \Phi_0$  from  $\sim 300$  to  $\sim 85 \text{ mV}$  is observed at  $\Phi_0 \approx 6 \times 10^{12} \text{ cm}^{-2} \text{ s}^{-1}$ . Remember that a similar decrease of  $dV_{oc}/d \log \Phi_0$  from  $\sim 230$  to  $\sim 120 \text{ mV}$  at  $\Phi_0 \approx 5 \times 10^{11} \text{ cm}^{-2} \text{ s}^{-1}$  appeared in Figure 2.

### 3.4. Simulation of the Effect of Band Edge Displacement.

Interestingly, the model allows the prediction of the influence of surface treatments on the light intensity dependence of  $V_{oc}$ . In general, a surface modification of the electrode leading to a decrease of the density of both shallow traps ( $\Theta_t$ ) and deep traps ( $N_t$ ) will produce an increase of  $V_{oc}$  at low and intermediate values of  $\Phi_0$ , but not at high illumination intensities, where recombination is controlled by interfacial electron transfer from cb states. On the other hand, a surface treatment leading to a shift of the cb edge,  $E_c$ , with respect to the electrolyte redox level,  $E_{redox}$ , will affect the recombination process involving both shallow and deep traps, as well as cb states. Figure 8 illustrates the influence of  $(E_c - E_{redox})$  on the  $\Phi_0$  dependence of  $V_{oc}$ . In general, the increase of  $(E_c - E_{redox})$  produces an increment of  $V_{oc}$  ( $\Delta V_{oc}$ ) in the whole range of  $\Phi_0$ . Moreover, for constant  $\Phi_0$ ,  $\Delta V_{oc}$  increases with  $(E_c - E_{redox})$  in the illumination range where recombination is controlled by band-gap ss. Only at high enough values of  $\Phi_0$ , where interfacial electron transfer from cb states dominates recombination, is  $dV_{oc}/d \log \Phi_0 \approx 60 \text{ mV}$  for any value of  $(E_c - E_{redox})$ ; that is, a parallel shift of the linear plot of  $V_{oc}$  vs  $\log \Phi_0$  takes place when  $(E_c - E_{redox})$  is changed. It is interesting to realize that for  $(E_c - E_{ox}) > (E_t - E_{ox})$  recombination is controlled by deep traps in the low  $\Phi_0$  range. In contrast, when  $(E_c - E_{ox}) < (E_t - E_{ox})$ , shallow traps

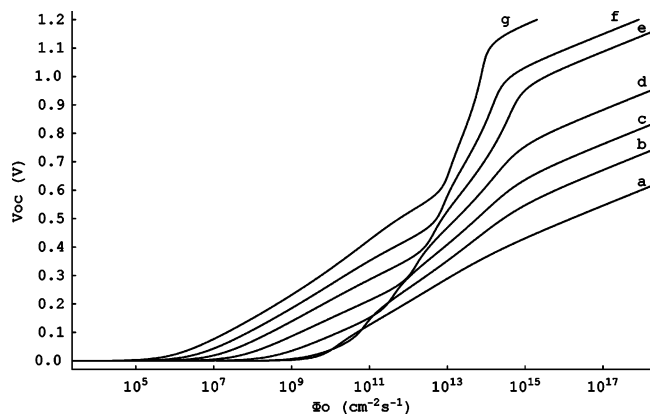


**Figure 8.** Effect of shifting the sc band edge,  $E_c$ , with respect to electrolyte redox level,  $E_{\text{redox}}$ , on the plot of  $V_{\text{oc}}$  vs  $\Phi_0$ . The shift is represented for the following values of  $E_c - E_{\text{redox}}$ : (a) 0.6 eV, (b) 0.7 eV, (c) 0.8 eV, (d) 0.9 eV, (e) 1.0 eV, (f) 1.1 eV, and (g) 1.2 eV.

dominate recombination for both low and intermediate  $\Phi_0$  values. Summing up, an increment of  $(E_c - E_{\text{ox}})$  associated with either a change of the electrolyte redox potential or a modification of the  $\text{TiO}_2$  surface leads, in general, to an increase of  $V_{\text{oc}}$ . More details and simulations showing these effects are provided in Figure S2 of the Supporting Information. Schlichthröl et al.<sup>9</sup> have found that in the illumination range  $10^{16} > \Phi_0 > 10^{13} \text{ cm}^{-2} \text{ s}^{-1}$  the plot of  $V_{\text{oc}}$  vs  $\log \Phi_0$  is linear ( $dV_{\text{oc}}/d \log \Phi_0 \approx 90 \text{ mV}$ ). These authors have also reported that the specific chemical surface treatment of the  $\text{TiO}_2$  dye-sensitized electrode with TBP and  $\text{NH}_3$  leads to a constant increase of  $V_{\text{oc}}$  ( $\Delta V_{\text{oc}} \approx 100 \text{ mV}$ ) in the whole range of  $\Phi_0$  (i.e.,  $dV_{\text{oc}}/d \log \Phi_0$  remains constant). The authors attribute this behavior to a photoinduced band edge movement leading to an increase of  $E_c - E_{\text{redox}}$ . Since an increment of  $E_c - E_{\text{redox}}$  produces an increase of  $dV_{\text{oc}}/d \log \Phi_0$  in the  $\Phi_0$  range where recombination is dominated by the tail of shallow traps and this is not observed by Schlichthröl et al., it may be inferred that a decreased  $\Theta_t$  (total density of ss) and/or  $A$  (the preexponential factor of the electron transfer rate  $e_{\text{ox}}$ , which is related to the degree of interaction of ss with redox electrolyte species) is involved in the observed increase of  $V_{\text{oc}}$ .

Another source of band edge shifts is the charging of the  $\text{TiO}_2$  particles with electrons and concomitant increase of ionic charge at the Helmholtz layer. The amount of band edge shift depends on the density of electrons and the value of the Helmholtz capacitance and may become significant at high light intensities. We have not considered this effect in detail in the present work, but from the above analysis, some insight on the effect of the shift due to electron accumulation can be obtained. In fact, it should produce a progressive displacement of the band edge, so that the light intensity dependence of  $V_{\text{oc}}$  should change in the direction of a  $\rightarrow$  g of Figure 8.

#### 4. Conclusions and Implications of the Model

In this paper, we have presented a model for the intensity dependence of the photovoltage in DSSCs that describes for the first time the complex experimental behavior observed for a large window of light intensities (6 orders of magnitude). Previously, much simpler models described the photovoltage in a restricted illumination range where a simple exponential dependence of  $V_{\text{oc}}$  on  $\Phi_0$  is found. Our model provides a physically plausible interpretation for the detailed features of the experimental curves (drastic slope changes) and constitutes a steady-state approach addressing the main characteristics of the DSSC. A main disadvantage of our model is the large number of adjustable parameters involved, so that, unless

independent measurements of some of them are made (e.g., the broadening parameter in the trap distribution), the value of the fitting becomes small. The application of the model to the calibration of other measurable kinetic parameters would be helpful for its further validation. This is the case for the electron lifetime, as it has been shown recently.<sup>22</sup>

Let us summarize the main features of the model at the present stage. Interfacial electron transfer is considered to take place via an indirect, two-step process involving band-gap ss. In the first step, cb electrons are trapped inelastically at band-gap ss; further, trapped electrons are either detrapped back to the cb or transferred isoenergetically to the electrolyte in a process of recombination with photogenerated holes ( $\text{I}_3^-$  species). In agreement with others authors,<sup>11–20</sup> two kinds of band-gap ss are involved in these processes, monoenergetic deep traps ( $N_t \approx 10^{15}–10^{16} \text{ cm}^{-3}$ ) at about 0.6 V below the cb edge and a tail (exponential distribution) of shallow traps just below  $E_c$  ( $\Theta_t \approx 10^{18}–10^{19} \text{ cm}^{-3}$ ;  $\alpha' = 0.3–0.5$ ). Note that a density of  $\Theta_t = 2 \times 10^{19} \text{ cm}^{-3}$  has been determined independently by cyclic voltammetry in experiments in aqueous solution.<sup>23</sup> According to eqs A1.5 and A1.6, under open-circuit conditions and low illumination intensities ( $10^{11} \leq \Phi_0 \leq 10^{12} \text{ cm}^{-2} \text{ s}^{-1}$ ), interfacial electron transfer mainly takes place via deep traps, and  $V_{\text{oc}}$  depends on the trap filling factor,  $f$ . For small values of  $f$ , the recombination rate via deep traps increases rapidly with  $\Phi_0$  and saturates for  $f \approx 1$ . As can be seen in Figure 2, this situation takes place for  $\Phi_0 \approx N_t e_{\text{ox}} = 1.45 \times 10^{11} \text{ cm}^{-2} \text{ s}^{-1}$ . For  $\Phi_0 > 10^{11}–10^{12} \text{ cm}^{-2} \text{ s}^{-1}$ , the recombination process starts to be controlled by the exponential distribution of ss (shallow traps). Finally, for high enough light intensities ( $\Phi_0 \geq 10^{15} \text{ cm}^{-2} \text{ s}^{-1}$ ), as long as  $n_0 e_{\text{ox}}^{\text{cb}} > \int_{E_{\text{redox}}}^{E_{\text{Fn}}} N_t(E) e_{\text{ox}}(E) dE$ , direct recombination via cb states becomes the dominant recombination mechanism, so that a linear dependence of  $V_{\text{oc}}$  on  $\log \Phi_0$ , with a slope of  $\sim 60 \text{ mV}$  (i.e.,  $\beta' = 1$  in eq 3), appears.

Summing up, at low enough illumination intensities, the dependence of  $V_{\text{oc}}$  on  $\Phi_0$  becomes controlled by localized, deep band-gap traps; for intermediate photon fluxes, the photovoltage is controlled by the tail of shallow band-gap traps; and for high enough  $\Phi_0$  values, cb states dominate the recombination process. The second and third stages are in agreement with the electron lifetime obtained by photovoltage decay measurements.<sup>22</sup> Because of the limited sensitivity of this technique, the first stage, associated with the deep surface states, cannot be detected.

While the energy of monoenergetic deep traps seems to be intrinsic to the nanostructured  $\text{TiO}_2$  material, their concentration,  $N_t$ , as well as the density,  $\Theta_t$ , and the distribution of shallow traps,  $\alpha'$ , change from sample to sample and are quite sensitive to the electrode preparation.

Although the photovoltage is very sensitive to the presence of band-gap ss, it must be emphasized that the maximum photovoltage reached by the DSSC under high enough light intensities,  $V_{\text{oc,max}} = E_c^* - E_{\text{redox}}$ , where  $E_c^*$  refers to the cb edge under illumination,<sup>24</sup> must not be affected by the presence of band-gap traps.

**Acknowledgment.** J.B. acknowledges the support of this work by Ministerio de Educación y Ciencia under project MAT2004-05168. A.Z. acknowledges the support of this work by the Israeli Ministry of Infrastructure. M.G.H. is grateful to CICYT (Spain) for generous support under Grant TIC2001-0931.

#### Appendix 1

We consider the solution of the rate eq 8 for localized, monoenergetic ss. First we note the relationship<sup>5</sup>

$$\frac{e_{\text{ox}}}{e_{\text{red}}} = \frac{c_{\text{ox}}}{c_{\text{red}}} \exp[(E_t - E_{\text{redox}})/kT] \quad (\text{A1.1})$$

Under equilibrium conditions in the dark, eq 9 becomes  $r_{t_0} = N_t(1 - f_0)e_{t_0}$ , with  $e_{t_0} \equiv e_{\text{tr}} = \sigma_n \nu n_0 = e_t(n_0/n)$  and  $r_t = r_{t_0} = N_t f_0 e_r$ . It can be shown that<sup>5</sup>

$$e_r = e_{t_0} \exp[(E_t - E_{\text{redox}})/kT] \quad (\text{A1.2})$$

so that by combining eqs A1.1 and A1.2 the following relationship between  $e_{t_0}$ ,  $e_r$ ,  $e_{\text{ox}}$ , and  $e_{\text{red}}$  is obtained:

$$\frac{e_r}{e_{t_0}} = \frac{e_{\text{ox}} c_{\text{red}}}{e_{\text{red}} c_{\text{ox}}} \quad (\text{A1.3})$$

On the other hand, from eq 8 we obtain<sup>5</sup>

$$n = n_0 \left[ \frac{(e_{\text{ox}} + e_r)f - e_{\text{red}}(1 - f)}{e_{t_0}(1 - f)} \right] \quad (\text{A1.4})$$

and

$$f = \frac{G + N_t e_{\text{red}}}{N_t(e_{\text{ox}} + e_{\text{red}})} \quad (\text{A1.5})$$

Finally, by combining eqs A1.4 and A1.5, it can be written that

$$\frac{n}{n_0} = \frac{e_{\text{ox}} + e_r}{e_{t_0}} \frac{G + N_t e_{\text{red}}}{N_t e_{\text{ox}} - G} - \frac{e_{\text{red}}}{e_{t_0}} \quad (\text{A1.6})$$

which, according to eq 4, leads to the relationship between  $V_{\text{oc}}$  and  $G(\Phi_0)$  stated in eq 13.

## Appendix 2

Since the integrand of eq 18 can be written as

$$N_t(E) e_{\text{ox}}(E) = \frac{A\alpha'\Theta_t}{kT} \exp\left(\frac{\alpha'(E - E_c)}{kT} - \frac{(E - E_{\text{ox}})^2}{4\lambda kT}\right) = \frac{A\alpha'\Theta_t}{kT} \exp C_1 \exp\left(-\frac{[E - (E_{\text{ox}} + 2\lambda\alpha')]^2}{4\lambda kT}\right) \quad (\text{A2.1})$$

where  $C_1 = (4\alpha'E_{\text{ox}}/4kT) + (4\lambda\alpha'^2/4kT) - (\alpha'/kT)E_c$ , by combining eqs 15–18 and A2.1 and taking  $E_{\text{redox}}$  as the energy origin, eq 15 becomes

$$G = \frac{A_{\text{ox}}\alpha'\Theta_t}{kT} \exp C_1 \times \int_0^{V_{\text{oc}}} \exp\left(-\frac{[(E - E_{\text{redox}}) - (E_{\text{ox}} + 2\lambda\alpha')]^2}{4\lambda kT}\right) dE \quad (\text{A2.2})$$

where the integrand is a Gaussian function with a mean value  $\mu = E_{\text{ox}} + 2\lambda\alpha'$  and a typical deviation  $\sigma = (2kT\lambda)^{1/2}$ . Therefore, the product of the exponential and Gaussian distribution of states results in a maximum of the combined density of states at  $2\lambda\alpha'$  above the  $E_{\text{ox}}$  level. Obviously, eq 15 can be related with the error function  $\text{erf}(x) = (2/\sqrt{\pi}) \int_0^x e^{-t^2} dt$ , so that it can be rewritten

$$G = C \left[ \text{erf}\left(\frac{a}{\sqrt{b}}\right) + \text{erf}\left(\frac{V_{\text{oc}} - a}{\sqrt{b}}\right) \right] \quad (\text{A2.3})$$

with  $C = (A_{\text{ox}}\alpha'\Theta_t\sqrt{\pi}/2kT) \exp C_1$ ,  $a = E_{\text{ox}} + 2\lambda\alpha'$ , and  $b = 4kT\lambda$ .

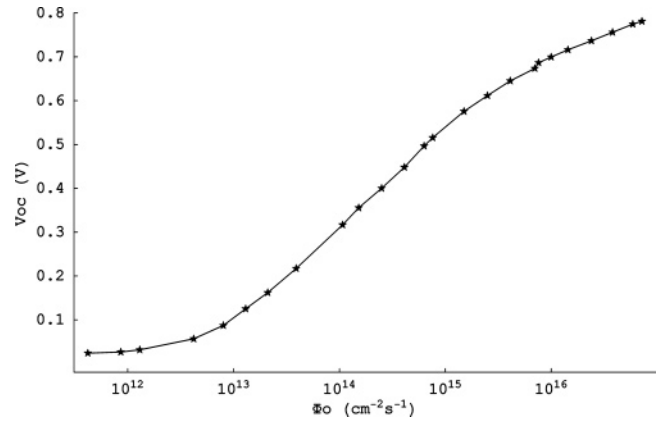


**Figure 9.** Photon flux dependence of the photovoltage for a DSSC analogous to that described in the Experimental Section, where the FTO conducting glass supporting the nanoporous TiO<sub>2</sub> film was substituted by a Ti sheet. The use of a Ti substrate provides natural blocking of the conductive substrate–electrolyte interface as a TiO<sub>2</sub> film about 2 nm thick is spontaneously formed at the Ti surface upon exposure to ambient conditions.

By applying the inverse of the error function to eq A2.3, we obtain the explicit dependence of  $V_{\text{oc}}$  on  $G$  that is given in eq 19.

## Appendix 3

Here, we present experimental results comparing the dependence of  $V_{\text{oc}}$  on  $\Phi_0$  for a DSSC in which the FTO substrate is substituted by a Ti substrate. The use of a Ti substrate provides natural blocking of the conductive substrate–electrolyte interface as TiO<sub>2</sub> is spontaneously formed at the Ti surface upon exposure to ambient conditions. For the fabrication of the Ti based electrodes, we used the procedure described in the Experimental Section except that a Ti plate was used as a substrate instead of the FTO glass. Treatment of the Ti plate and the formation of the TiO<sub>2</sub> at the Ti surface under the sintering conditions are reported elsewhere.<sup>25</sup> Figure 9 shows the experimental  $\Phi_0(V_{\text{oc}})$  plot corresponding to a Ti based DSSC, i.e., where a native TiO<sub>2</sub> blocking layer exists at the substrate–electrolyte interface. Except for effects related to the illumination via the counter electrode, the shape of the curve is similar to those corresponding to FTO based DSSCs.

In the following, we compare our results with those reported by Peter et al.<sup>6,7</sup> The differences observed will be analyzed in light of both Peter's model<sup>6</sup> and the model presented here.

Let us first analyze the influence of the back-reaction of electrons via the substrate on the photon flux dependence of the photovoltage. The rate of this reaction can be expressed by the Butler–Volmer equation, in terms of the photovoltage, as<sup>6</sup>

$$U_{\text{sub}} = -j_0 \left[ \exp \frac{\beta n q V_{\text{oc}}}{kT} - \exp \frac{(1 - \beta) q V_{\text{oc}}}{kT} \right] \quad (\text{A3.1})$$

where  $j_0$  represents the exchange current density,  $\beta$  and  $(1 - \beta)$  are the anodic and cathodic transfer coefficients, respectively, and  $n$  is the number of electrons participating in the electroreduction of tri-iodide ions. Therefore, according to our model, the general dependence of  $V_{\text{oc}}$  on  $\Phi_0$  will be obtained by addition of the term  $U_{\text{sub}}$  given by eq A3.1 to eq 20. Obviously, eq A3.2

$$\Phi_0(V_{\text{oc}}) = U_{\text{ss},1}(V_{\text{oc}}) + U_{\text{ss},2}(V_{\text{oc}}) + U_{\text{cb}}(V_{\text{oc}}) + U_{\text{sub}}(V_{\text{oc}}) \quad (\text{A3.2})$$

and eq 20 will give identical values of  $\Phi_0(V_{\text{oc}})$  if  $U_{\text{sub}}(V_{\text{oc}})$  is

**TABLE 1: Comparison Test of our FTO Based DSSCs with Those of Fisher et al.<sup>7</sup> and Cameron et al.,<sup>6</sup> Attending to the Following Parameters: Photon Flux for the Photovoltage Onset ( $\Phi_{0,\text{on}}$ ), Maximum Attained Photovoltage ( $V_{\text{oc,max}}$ ), the Corresponding Photon Flux ( $\Phi_{0,\text{max}}$ ), and the Inflection of  $dV_{\text{oc}}/d \log \Phi_0$  at Low Photon Flux**

DSSC	$\Phi_{0,\text{on}}$ ( $\text{cm}^{-2} \text{s}^{-1}$ )	$V_{\text{oc,max}}$ (V)	$\Phi_{0,\text{max}}$ ( $\text{cm}^{-2} \text{s}^{-1}$ )	$dV_{\text{oc}}/d \log \Phi_0$ inflection at low $\Phi_0$
bare electrode	$5 \times 10^{10}$	This Paper $\sim 0.6$	$2 \times 10^{15}$	existing at: $\Phi_0 \approx 2 \times 10^{11} \text{ cm}^{-2} \text{ s}^{-1}$ $\Phi_0 \approx 2 \times 10^{11} \text{ cm}^{-2} \text{ s}^{-1}$
PPO coated electrode	$5 \times 10^{10}$	$\sim 0.6$	$2 \times 10^{15}$	
bare electrode	$10^{11}$	Fisher et al. $\sim 0.6$	$6 \times 10^{15}$	existing at: $\Phi_0 = 3 \times 10^{12} \text{ cm}^{-2} \text{ s}^{-1}$
bare electrode	$5 \times 10^{13}$	Cameron et al. $\sim 0.6$	$10^{17}$	nonexisting
coated electrode	nonreported	$\sim 0.6$	$10^{17}$	nonreported

negligible with respect to  $U_{\text{ss},1}(V_{\text{oc}})$ ,  $U_{\text{ss},2}(V_{\text{oc}})$ , and  $U_{\text{cb}}(V_{\text{oc}})$ , something that frequently occurs in practice, as we are going to show. Figure 10a shows a plot of the term  $U_{\text{sub}}(V_{\text{oc}})$  for different values of the exchange current density  $j_0$ , which varies between  $10^{-9}$  and  $10^{-5} \text{ A cm}^{-2}$ , together with the  $\Phi_0(V_{\text{oc}})$  plot of Figure 2 (full line) corresponding to the best fitting of our model (eq 20) to the experimental data of Figure 2. In Figure 10b, we represent  $\Phi_0(V_{\text{oc}})$  according to eq A3.2 for the different values of  $j_0$  represented in Figure 10a. It can be seen that for  $j_0 \leq 10^{-9} \text{ A cm}^{-2}$  the influence of the term  $U_{\text{sub}}$  is negligible even at low light intensities, which means that under such experimental conditions no significant differences should exist between experimental values corresponding to a DSSC with and without blocking of the FTO–electrolyte contact, as, in fact, observed

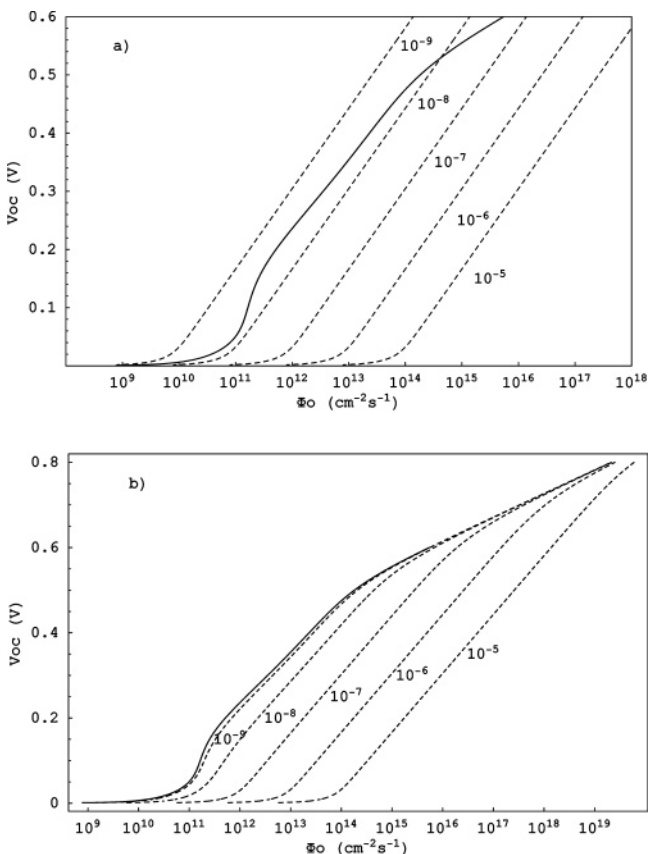


**Figure 10.** (a) Plot of the transfer rate of electrons from the FTO substrate to electrolyte tri-iodide ions according to eq A3.1 (Appendix 3), for  $\beta = 0.5$  and different values of the exchange current density,  $j_0$ . The plot of  $\Phi_0(V_{\text{oc}})$  corresponding to the best fitting of eq 29 to the experimental data of Figure 2 is also included (full line). (b) Plot of eq A3.2 (Appendix 3) for the different values of  $U_{\text{sub}}(V_{\text{oc}})$  in part a.

experimentally in Figure 2. Observe that the actual value of  $j_0$  could be even lower than  $10^{-9} \text{ A cm}^{-2}$  because a considerable fraction of the FTO substrate is covered with  $\text{TiO}_2$  nanoparticles and the actual area in contact with the electrolyte is much less than the geometric electrode area.

Let us now analyze the main differences between our model and that of Cameron et al.<sup>6</sup> First, these authors do not consider the existence of monoenergetic deep traps participating as surface recombination centers but only the existence of an exponential distribution of shallow traps. Second, they use a global first-order rate constant,  $k_{\text{ss}}$ , for electron transfer from surface states to the electrolyte, without taking into account that the Marcus–Gerischer model predicts a  $k_{\text{ss}}$  dependent not only on the reorganization energy of the system ( $\lambda$ ) but also on the free energy difference,<sup>5</sup> as taken into account by eqs 16–18 of our model. The influence of these differences on the  $V_{\text{oc}}(\Phi_0)$  behavior is significant, mainly with respect to the dependence of  $dV_{\text{oc}}/d \log \Phi_0$  on  $\Phi_0$  at low  $\Phi_0$  values. In fact, according to the model of Cameron et al. (see Figures 2–4 of ref 6), at low enough values of  $\Phi_0$ ,  $dV_{\text{oc}}/d \log \Phi_0$  increases monotonically with  $\Phi_0$  and then reaches a constant value which depends on the value of the parameters  $\beta$ ,  $n$ , and  $\alpha'$ . In contrast, when according to our model recombination via deep traps is taken into account, an inflection must appear at low enough illumination flux in the plot of  $dV_{\text{oc}}/d \log \Phi_0$  vs  $\Phi_0$ . Actually, as far as the term  $U_{\text{ss},1}$  of eq 20, associated with deep traps, controls the recombination process at low photon flux,  $dV_{\text{oc}}/d \log \Phi_0$  increases monotonically with  $\Phi_0$ . However, as  $\Phi_0$  increases and recombination via shallow traps is the prevailing process (i.e.,  $U_{\text{ss},1} \ll U_{\text{ss},2}$ ),  $dV_{\text{oc}}/d \log \Phi_0$  stops increasing and starts to decrease. This is just the behavior observed in Figure 2 and Figure S1 of the Supporting Information for values of  $\Phi_0$  of about  $10^{11}$  and  $10^{12} \text{ cm}^{-2} \text{ s}^{-1}$ , respectively.

Finally, it is instructive to compare in Figure 11 the different  $V_{\text{oc}}$  vs  $\Phi_0$  experimental data considered here (our own data and those of Peter and collaborators<sup>6,7</sup>). The results of this comparison, which mainly concerns the photon flux for the onset of photovoltage ( $\Phi_{0,\text{on}}$ ), the maximum reached photovoltage ( $V_{\text{oc,max}}$ ) with the corresponding photon flux ( $\Phi_{0,\text{max}}$ ), and the inflection of  $dV_{\text{oc}}/d \log \Phi_0$  at low enough values of  $\Phi_0$ , are reviewed in Table 1. The following points are remarkable: (1) our DSSCs are not sensitive to the blocking treatment of the FTO substrate, which contrasts with the behavior shown by the DSSC of Cameron et al.<sup>6</sup> (the  $V_{\text{oc}}$  vs  $\Phi_0$  curve is noticeably shifted toward high  $\Phi_0$  values when the FTO–electrolyte contact is blocked); (2) an inflection of  $dV_{\text{oc}}/d \log \Phi_0$  at low  $\Phi_0$  values is observed for our DSSCs, with and without blocking of the substrate–electrolyte interface, as well as for the uncoated sample of Fisher et al.;<sup>7</sup> this is not reported for the bare electrode

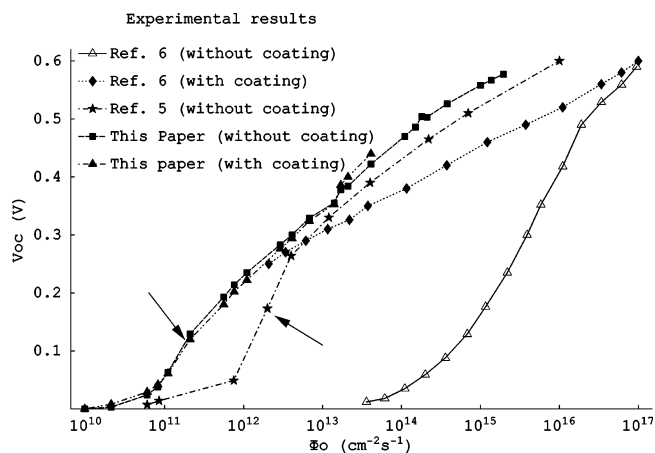


**Figure 11.** Comparison of the  $V_{oc}$  vs  $\Phi_0$  curves corresponding to our FTO based DSSCs in Figure 2 with those reported by Peter and collaborators in refs 6 and 7. The arrows indicate the inflection of  $dV_{oc}/d \log \Phi_0$  at low enough values of  $\Phi_0$  that according to our model indicates interfacial recombination via localized, band-gap deep traps. Observe that this inflection cannot be observed in the FTO coated sample of ref 6 due to the lack of  $V_{oc}$  experimental data for low enough illumination intensity (the lowest reported photovoltage is about 0.25 V). In contrast, the absence of inflection for the FTO uncoated sample of ref 6 is attributed to the dominant effect of FTO substrate in the whole interfacial recombination process ( $U_{sub}(V_{oc}) \gg U_{ss,1}(V_{oc})$ ).

used by Cameron et al.;<sup>6</sup> (3) the  $V_{oc}$  vs  $\Phi_0$  performance of the DSSC is not necessarily improved by intentionally blocking the FTO–electrolyte contact. These differences must be attributed, at least partially, to the type of FTO substrate used. While our DSSC and that of Fisher et al.<sup>7</sup> used a Libby Owens Ford FTO as the substrate, that of Cameron et al. (Figure 9 of ref 6) was prepared with a FTO from Asahi. Moreover, the FTO substrate used by Cameron et al.<sup>6</sup> was ultracleaned (sonicated in 5% Deconex solution, thoroughly rinsed, and further cleaned by sonication in 2-propanol and ethanol), in comparison with the cleaning performed by us and Fisher et al. (simple immersion in a solution of KOH in 2-propanol and further rinsing in deionized water). In consequence, the electrochemical activity of the FTO substrate used by Cameron et al. could be much higher than that of the one used by us and Fisher et al. In fact, as shown in Figure 11, the behavior of our electrode (not affected by the blocking treatment) is compatible with a relatively small  $j_0$  value ( $\leq 10^{-8}$  A cm<sup>-2</sup>). A low exchange current density may also be valid for the Fisher et al. FTO substrate. In contrast, the strong behavior difference observed in Figure 11 between the bare and the coated electrode of Cameron et al. should be consistent with a  $j_0$  value several orders of magnitude higher for their ultracleaned FTO substrate.

### Notation

$A_{ox}$  = interfacial exchange probability of electrons from band-gap ss to I<sub>2</sub> oxidized electrolyte species (s<sup>-1</sup>)  
 $A_{red}$  = interfacial exchange probability of electrons from I<sub>3</sub><sup>-</sup> reduced electrolyte species to band-gap ss (s<sup>-1</sup>)  
 $D$  = diffusion coefficient for cb electrons (cm<sup>-2</sup> s<sup>-1</sup>)  
 $E$  = band-gap ss energy (eV)  
 $E_c$  = bottom cb level energy (eV)  
 $E_{Fn}^*$  = quasi-Fermi level energy (eV)  
 $E_{ox}$  = most probable energy level for oxidized electrolyte species (eV)  
 $E_{red}$  = most probable energy level for reduced electrolyte species (eV)  
 $E_{redox}$  = electrolyte redox energy (eV)  
 $G$  = cb electrons photogeneration rate (cm<sup>-3</sup> s<sup>-1</sup>)

$N_c$  = effective density of free cb electrons (cm<sup>-3</sup>)  
 $N_t$  = density of monoenergetic, deep band-gap ss (cm<sup>-3</sup>)  
 $T_c$  = characteristic temperature of exponential distribution of shallow band-gap ss (K)

$U_{cb}$  = recombination rate of interfacial transfer of electrons from the cb to the electrolyte (cm<sup>-3</sup> s<sup>-1</sup>)

$U_{ss,1}$  = recombination rate of interfacial transfer of electrons from localized, band-gap deep traps to the electrolyte (cm<sup>-3</sup> s<sup>-1</sup>)

$U_{ss,2}$  = recombination rate of interfacial transfer of electrons from the exponential distribution of shallow band-gap ss to the electrolyte (cm<sup>-3</sup> s<sup>-1</sup>)

$U_{sub}$  = recombination rate of interfacial transfer of electrons from the substrate to the electrolyte (cm<sup>-3</sup> s<sup>-1</sup>)

$V_{oc}$  = photovoltage (volts)

$c_{ox}$  = electrolyte concentration of I<sub>2</sub> oxidized species (cm<sup>-3</sup>)

$c_{red}$  = electrolyte concentration of I<sub>3</sub><sup>-</sup> reduced species (cm<sup>-3</sup>)

$d$  = nanostructured TiO<sub>2</sub> film thickness (cm)

$e_{ox}$  = interfacial transfer frequency of electrons from band-gap ss to I<sub>2</sub> oxidized electrolyte species (s<sup>-1</sup>)

$e_{red}$  = interfacial transfer frequency of electrons from I<sub>3</sub><sup>-</sup> reduced electrolyte species to band-gap ss (s<sup>-1</sup>)

$e_r$  = frequency of detrapping of electrons from band-gap ss to the cb (s<sup>-1</sup>)

$e_t$  = frequency of trapping of cb electrons by band-gap ss under illumination (s<sup>-1</sup>)

$e_{t0}$  = frequency of trapping of cb electrons by band-gap ss under equilibrium conditions in the dark (s<sup>-1</sup>)

$f$  = filling factor of band-gap ss (dimensionless)

$j_0$  = substrate exchange current density (A cm<sup>-2</sup>)

$n$  = concentration of cb electrons under illumination (cm<sup>-3</sup>)

$n_0$  = concentration of cb electrons under equilibrium conditions in the dark (cm<sup>-3</sup>)

$q$  = electron charge

$r_{ox}$  = rate of interfacial transfer of electrons from band-gap ss to oxidized electrolyte species (cm<sup>-3</sup> s<sup>-1</sup>)

$r_{red}$  = rate of interfacial transfer of electrons from reduced to reduced electrolyte species to band-gap ss (cm<sup>-3</sup> s<sup>-1</sup>)

$r_r$  = rate of detrapping of electrons from band-gap ss to the cb (cm<sup>-3</sup> s<sup>-1</sup>)

$r_t$  = trapping rate of cb electrons by band-gap ss (cm<sup>-3</sup> s<sup>-1</sup>)

$\alpha$  = absorptivity of the nanostructured TiO<sub>2</sub> film (cm<sup>-1</sup>)

$\alpha'$  = broadening parameter defining the exponential distribution of shallow band-gap ss (dimensionless)

$\beta$  = anodic transfer coefficient of the substrate (dimensionless)

$\beta'$  = recombination reaction order in the concentration of cb electrons (dimensionless)

$\lambda$  = reorganization energy according to Gerischer's model (eV)

$\nu$  = thermal velocity of cb electrons (cm s<sup>-1</sup>)

$\sigma_n$  = electron capture cross section of band-gap ss (cm<sup>2</sup>)

$\Phi_0$  = incident illumination flux (cm<sup>-2</sup> s<sup>-1</sup>)

$\Theta_t$  = density of shallow band-gap ss (cm<sup>-3</sup> s<sup>-1</sup>)

**Supporting Information Available:** Fitting of  $V_{oc}$  vs  $\Phi_0$  of the experimental data of Fisher et al.<sup>7</sup> with our recombination model, details on the simulation given in Figure 8, and table of related values. This material is available free of charge via the Internet at <http://pubs.acs.org>.

### References and Notes

- (1) O'Regan, B.; Grätzel, M. *Nature* **1991**, *353*, 737.
- (2) Usami, A.; Ozaki, H. *J. Phys. Chem. B* **2001**, *105*, 4577–4583.

- (3) Peter, L. M.; Duffy, N. W.; Wang, R. L.; Wijayantha, K. G. U. *J. Electroanal. Chem.* **2002**, 524–525, 127.
- (4) Bisquert, J.; Vikhrenko, V. S. *J. Phys. Chem. B* **2004**, 108, 2313.
- (5) Bisquert, J.; Zaban, A.; Salvador, P. *J. Phys. Chem. B* **2002**, 106, 8774.
- (6) Cameron, P. J.; Peter, L. M.; Hore, S. *J. Phys. Chem. B* **2005**, 109, 930.
- (7) Fisher, A. C.; Peter, L. M.; Ponomarev, E. A.; Walker, A. B.; Wijayantha, K. G. U. *J. Phys. Chem. B* **2000**, 104, 949.
- (8) Cameron, P. J.; Peter, L. *J. Phys. Chem. B* **2003**, 107, 14394.
- (9) Schlichthörl, G.; Huang, S. Y.; Sprague, J.; Frank, A. J. *J. Phys. Chem. B* **1997**, 101, 8141.
- (10) Gerischer, H. Z. *Phys. Chem. NF* **1960**, 26, 233.
- (11) Boschloo, G.; Goossens, A. *J. Phys. Chem.* **1996**, 100, 19489.
- (12) Boschloo, G.; Fitzmaurice, D. *J. Phys. Chem. B* **1999**, 103, 2228.
- (13) Wang, H.; He, J.; Boschloo, G.; Lindström, H.; Hagfeldt, A.; Lindquist, S. I. *J. Phys. Chem. B* **2001**, 105, 2529.
- (14) Redmond, G.; Fitzmaurice, D.; Grätzel, M. *J. Phys. Chem.* **1993**, 97, 6951.
- (15) Usami, A.; Ozaki, H. *J. Phys. Chem. B* **2001**, 105, 4577.
- (16) Kay, A.; H-Baker, R.; Grätzel, M. *J. Phys. Chem.* **1994**, 98, 952.
- (17) van de Lagemaat, J.; Frank, A. J. *J. Phys. Chem. B* **2000**, 104, 4292.
- (18) Dloczik, L.; Ieperuma, O.; Lauerman, I.; Peter, L. M.; Ponomarev, E. A.; Redmond, G.; Shaw, N. J.; Uhlendorf, I. *J. Phys. Chem. B* **1997**, 101, 10281.
- (19) Nelson, J. *Phys. Rev. B* **1999**, 59, 15374.
- (20) Könenkamp, R. *Phys. Rev. B* **2000**, 61, 11057.
- (21) Marshall, J. M. *Rep. Prog. Phys.* **1983**, 46, 1235.
- (22) Bisquert, J.; Zaban, A.; Greenshtein, M.; Mora-Seró, I. *J. Am. Chem. Soc.* **2004**, 126, 13550.
- (23) Fabregat-Santiago, F.; Mora-Seró, I.; Garcia-Belmonte, G.; Bisquert, J. *J. Phys. Chem. B* **2003**, 107, 758.
- (24) Turrión, M.; Bisquert, J.; Salvador, P. *J. Phys. Chem. B* **2003**, 107, 9397.
- (25) Chappel, S.; Grinis, L.; Ofir, A.; Zaban, A. *J. Phys. Chem. B* **2005**, 109, 1643–1647.